Titania Coated Upconversion Nanoparticles for Near-Infrared Light Triggered Photodynamic Therapy

Sasidharan Swarnalatha Lucky,[†,‡] Niagara Muhammad Idris,[‡] Zhengquan Li,[§] Kai Huang,[‡] Khee Chee Soo,[⊥] and Yong Zhang*[,‡,∥]

[†]NUS Graduate School for Integrative Sciences & Engineering (NGS), Singapore 117456, [‡]Department of Biomedical Engineering, National University of Singapore, Singapore 117575, [§]Department of Materials Physics, Zhejiang Normal University, Jinhua 321004, PR China, [⊥]Division of Medical Sciences, National Cancer Centre Singapore, Singapore 169610, and [∥]College of Chemistry and Life Sciences, Zhejiang Normal University, Jinhua 321004, PR China

ABSTRACT Because of the limited penetration depth of visible light that generally excites most of the available photosensitizers (PSs), conventional photodynamic therapy (PDT) is limited to the treatment of superficial and flat lesions. Recently, the application of deep penetrating near-infrared (NIR) light excitable upconversion nanoparticles (UCNs) in conjunction with PDT has shown to have clear potential in the treatment of solid tumors due to its ability to penetrate thick tissue. However, various constructs developed so far have certain limitations such as poor or unstable PS loading, reducing their therapeutic efficacy and limiting their application to solution or cell-based studies. In this work, we present a method to fabricate uniform core–shell structured nanoconstruct with a thin layer of photocatalyst or PS–titanium dioxide (TiO_2) stably coated on individual UCN core. Our design allows controllable and highly reproducible PS loading, preventing any leakage of PS compared to previously developed nanoconstructs, thus ensuring repeatable PDT results. Further surface modification of the developed nanoconstructs with polyethylene glycol (PEG) rendered them biocompatible, demonstrating good therapeutic efficacy both *in vitro* and *in vivo*.

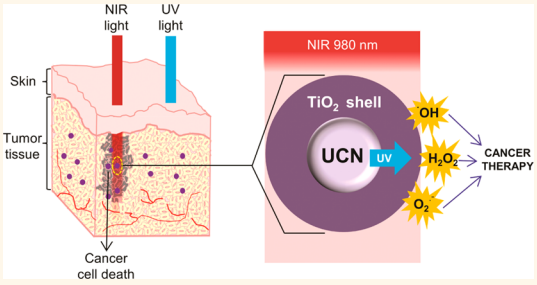

KEYWORDS: upconversion nanoparticles · titanium dioxide · photodynamic therapy · near-infrared · cancer

Photodynamic therapy (PDT) involves local or systemic administration of a photosensitizer (PS), followed by irradiation of the target lesion with light of a specific wavelength.[1] This triggers oxidative photodamage by the generation of reactive oxygen species (ROS), subsequently leading to direct tumor cell kill, vascular damage and activation of a nonspecific immune response.[2−6] It is a highly localized and minimally invasive therapeutic approach, with low systemic toxicity and fewer side effects as compared with chemo- and radiation therapy. However, at present it is not suitable for the treatment of solid tumors that are at a thickness greater than a few millimeters as most of the available PSs are activated by visible light (400−700 nm), which has limited penetration depth in tissues. Apparently, for deep penetration of light into tissues, wavelength of the irradiated beam should be in the near-infrared (NIR) window (700−1100 nm).[7] Recently, the use of upconversion nanoparticles (UCN) has opened a new avenue for tackling the shortcomings in this field. UCNs are "nanotransducers" that have the ability to convert low-energy NIR light to high energy visible or ultraviolet (UV) light, *via* an anti-Stokes emission process. In the recent years, there have been few studies on such UCN based PDT systems, in which an appropriate PS is closely attached to the UCN that act both as a "delivery agent" as well as NIR to visible/UV light "transducer", required for the activation of PS at much deeper levels in the tissues. The selection and attachment of PS to the UCN is of prime importance for the success of this technology. While a good overlap between the UCN emission and absorption maxima of the PS is required for efficient upconversion, sufficient amount of PS in close proximity to the UCN is necessary for efficient ROS generation. Previously, the three common strategies of PS loading on UCNs have been silica encapsulation, covalent conjugation and physical

* Address correspondence to biezy@nus.edu.sg.

Received for review June 25, 2014 and accepted October 21, 2014.

Published online January 07, 2015
10.1021/nn503450t

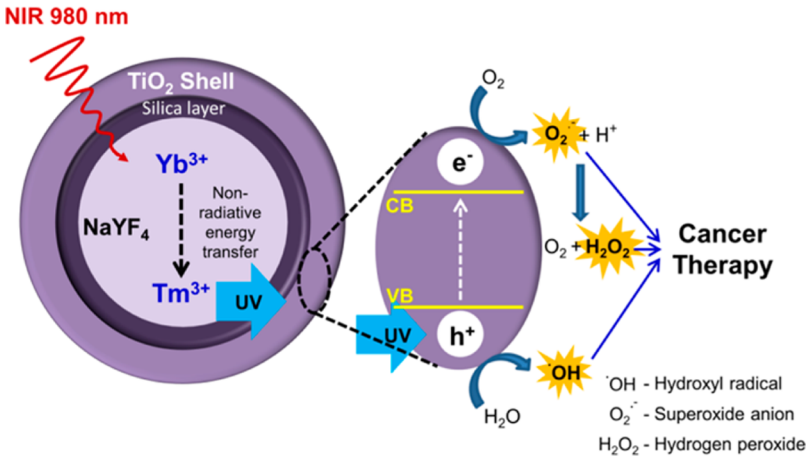

Scheme 1. Upon NIR irradiation, upconverted UV light emitted from $NaYF_4$:Yb,Tm UCN core photoexcites electrons in the valence band (VB) of the TiO_2 shell to the conduction band (CB), thus resulting in the formation of photoinduced hole-electron pairs. Interaction of electrons and holes with surrounding O_2 and H_2O molecules generate various ROS, eventually leading to cancer cell kill.

adsorption. While the widely adopted silica encapsulation (incorporation of PS in the silica or mesoporous silica shell) technique generally leads to relatively large sized particles with unstable PS loading,[8−12] covalent conjugation of PS is often associated with low PS loading efficiency.[13−16] On the other hand, physical adsorption method makes use of noncovalent hydrophobic forces allowing close binding of PS to the UCN core achieving the highest PS payload among the different constructs proposed until date.[17−20] However, none of these strategies guarantee controlled loading of PS or attachment of PS to the UCN, often compromising the repeatability of PDT results. Therefore, it becomes essential to design robust UCN constructs with controllable and stable PS loading, for optimal and reproducible therapeutic efficiency.

In this study, we report a different approach of uniformly surface coating a photocatalyst—titanium dioxide (TiO_2) on a $NaYF_4$:Yb,Tm UCN core (TiO_2-UCN) and demonstrate the ability of the synthesized nanoconstruct in achieving cancer cell kill both *in vitro* and *in vivo*. TiO_2, a well-studied photocatalyst, has been previously shown to have photokilling ability in variety of cancer cells *in vitro*[21−25] and *in vivo*[21,24,26] upon irradiation with UV light. However, direct excitation of TiO_2 nanoparticles by UV light suffer from limited penetration ability of UV light in the tissue (few fractions of a millimeter), making this technique only suitable for the treatment of superficial tumors.[26] Some effort to improve the penetration depth and thereby the PDT effect of TiO_2 has been recently reported by employing UCNs and fabricating nonuniform composite nanostructures with a few UCNs embedded in TiO_2 matrix.[27] However, the study mainly reported experiments conducted in solution and cell-based assays, perhaps due to the nonuniform size of the nanoconstruct that might have compromised repeatability and translatability of PDT results *in vivo*. Our design allows controllable and uniform PS (TiO_2) loading on individual UCN core and completely eliminates the possibility of PS leakage, thus ensuring significant ROS generation for effective and repeatable PDT results *in vitro* and *in vivo*. As illustrated in Scheme 1, the UCN core upconverts NIR light to UV light, which further photoexcites the electrons in the valence band (VB) of TiO_2 shell to conduction band (CB). This results in the formation of electron—hole pair eliciting further redox reactions for the generation of ROS.

Recently, we reported the synthesis of core—shell UCNs with thin and continuous layer of TiO_2, and further studied its stability in terms of ROS generation upon NIR excitation, in different storage conditions.[28] However, we observed saturation in its cell killing ability, such that the photocatalytic killing ability of the nanoparticles did not increase much with increase in concentration, and the maximum cell kill achieved was 50—60% under the best conditions. This could perhaps been due to the formation of large aggregates in the complex biological environment, hampering its effective uptake into the cells. In this study, we further surface modified the core—shell TiO_2-UCNs with polyethylene glycol (PEG) to impart stability and stealth properties, toward making it more conducive for biological applications. Its ability to induce cancer cell kill upon NIR excitation are tested both *in vitro* and *in vivo* to demonstrate the feasibility of utilizing this promising technology for treatment of solid tumors.

RESULTS AND DISCUSSION

Synthesis and Characterization of TiO_2-UCNs and Mal-PEG-TiO_2-UCNs. A hydrophobic $NaYF_4$:20%Yb,0.5%Tm UCN core was synthesized by solvent-thermal process. To impart hydrophilicity, UCN core was further coated with a thin layer of silica ($NaYF_4$:Yb,Tm @SiO_2) (Figure 1A). Subsequent grafting of (3-aminopropyl)-trimethoxysilane (APS) provided positively charged amino groups for

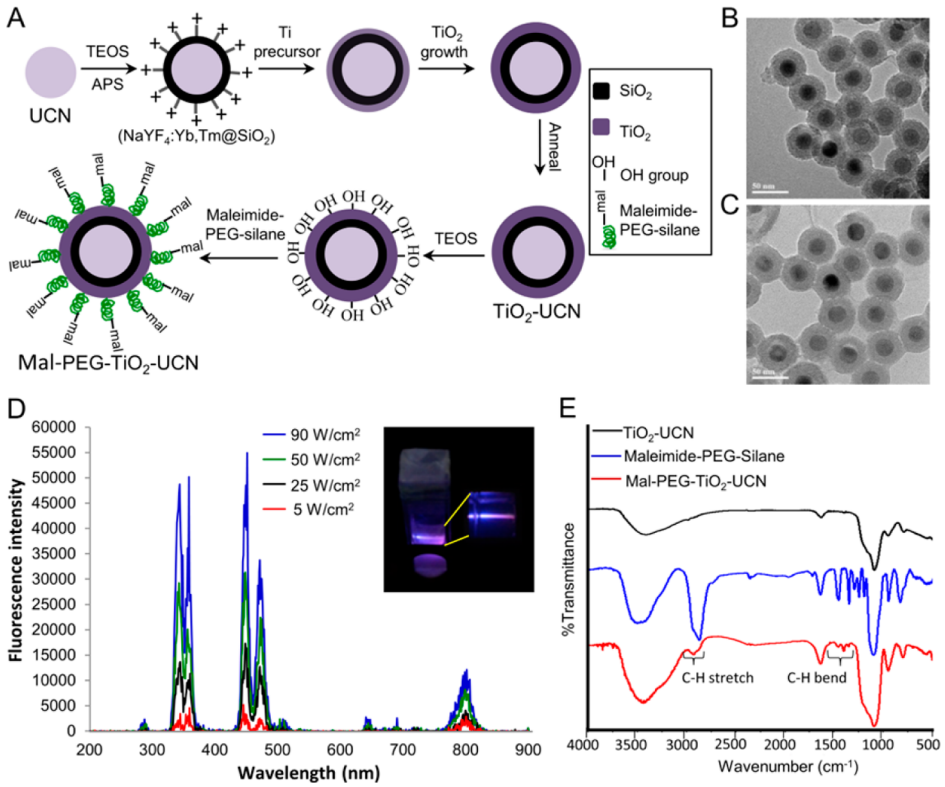

Figure 1. (A) Schematic of synthesis of TiO_2-UCN and Mal-PEG-TiO_2-UCN. TEM images of (B) TiO_2-UCNs and (C) Mal-PEG-TiO_2-UCN, (scale bar: 50 nm). (D) Fluorescence emission spectra of 100 μg/mL TiO_2-UCN in PBS under NIR excitation at different power densities (photon multiplier tube (PMT) voltage at 500 V); inset shows blue fluorescence emission from TiO_2-UCNs upon NIR excitation at 90 W/cm^2. (E) FT-IR absorption spectra of TiO_2-UCN, Maleimide-PEG-silane and Mal-PEG-TiO_2-UCN.

the binding of titanium precursor, followed by gradual epitaxial growth of the titanium precursor resulting in homogeneous coating of a thin layer of TiO_2 on UCN (TiO_2-UCN). Addition of tetraethyl orthosilicate (TEOS) conferred hydroxyl (OH) groups on the TiO_2 shell for the attachment of silane group of maleimide-PEG-silane, resulting in the formation of Mal-PEG-TiO_2-UCNs. Transmission electron microscopy (TEM) of both TiO_2-UCNs and Mal-PEG-TiO_2-UCNs revealed a uniform spherical shape with a well-defined core−shell structure and average primary particle size of ~50 nm (Figure 1B and 1C). The average diameter of the UCN core was ~25 nm that was surrounded by a silica layer and TiO_2 shell with a combined thickness of ~12.5 nm (Supporting Information, Figure S1A). Upon 980 nm NIR light irradiation, TiO_2-UCNs emitted upconverted light in UV, visible and NIR regions of the spectrum (Figure 1D and Supporting Information, Figure S1B). The UCN's blue emission (peaks at 450 and 475 nm) could be used to track the nanoparticles uptake by cells, whereas for *in vivo* imaging its emission at the NIR region (800 nm) could be utilized to capture signals from deeper tissues. Fourier transform infrared (FT-IR) absorption spectra confirmed successful grafting of maleimide-PEG-silane on the surface of TiO_2-UCN, with characteristic peaks of PEG appearing at ~2885 and ~1470−1350 cm^{-1} corresponding to C−H stretching and C−H bending respectively (Figure 1E).

Stability and ROS Generation of Nanoconstructs in Physiological Solutions. Initial studies using TiO_2-UCNs revealed formation of large aggregates (in the range of micrometres) in water and various physiological solutions at room temperature (RT) (Figure 2A and Supporting Information, Figure S2A,B). While it is known that hydrodynamic size of nanoparticles dispersed in liquid is often larger than its primary particle size as measured by TEM, here they seemed to increase substantially as a function of time and temperature (Supporting Information, Figure S2C) leading to rapid sedimentation of the aggregates. However, in RPMI-1640 medium (RPMI) with 10% fetal bovine serum (FBS), TiO_2-UCNs formed a stable dispersion. To check, if this was due to the presence of serum proteins, we compared the aggregation characteristic of TiO_2-UCNs in phosphate buffered saline (PBS) and PBS with 10% FBS, and found that there was over 10 time increase in particle size in the absence of FBS (Figure 2B and Supporting Information, Figure S2D).

To better understand the process of aggregation, the surface charge of these nanoparticles were studied by measuring the zeta-potential. When TiO_2 nanoparticles are dispersed in water, the surface of the nanoparticle is generally covered by hydroxyl group ($Ti^{IV} + H_2O \rightarrow Ti^{IV}-OH + H^+$),[29] which imparts a negative charge to it. As expected, although TiO_2-UCNs had a negative zeta-potential (Table 1), its value was

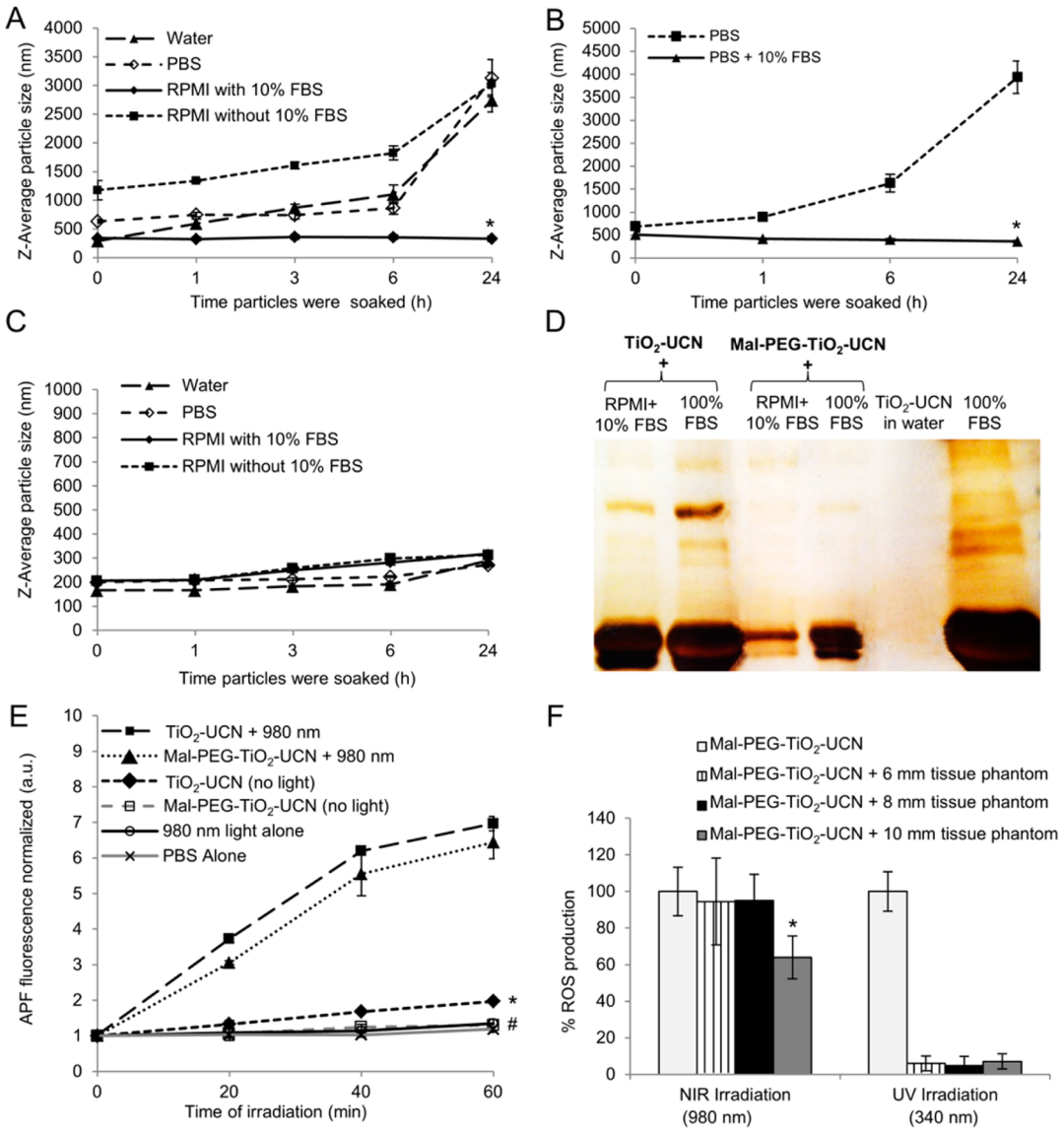

Figure 2. (A) Average hydrodynamic size of 100 μg/mL TiO_2-UCN soaked in different media at RT plotted as a function of time the nanoparticles were soaked, *$P < 0.0001$ *versus* size of TiO_2-UCNs in RPMI without FBS. (B) Effect of addition of 10% FBS on hydrodynamic size of 100 μg/mL TiO_2-UCN soaked in PBS, *$P < 0.0001$ compared to size of TiO_2-UCNs at 24 h. (C) Average hydrodynamic size of 100 μg/mL Mal-PEG-TiO_2-UCN in different solutions at RT plotted as a function of time. (D) Image of a silver stained gel to detect adsorption of serum proteins on the surface of nanoparticles suspended in either RPMI with 10% FBS or in 100% FBS. Unmodified TiO_2-UCN in water and 100% FBS were run as negative and positive controls, respectively. (E) Comparison of ROS production from nonirradiated and irradiated nanoparticles in PBS, *,#$P < 0.0001$ *versus* ROS production from nonirradiated TiO_2-UCNs and Mal-PEG-TiO_2-UCNs respectively after 60 min. Data are mean ($n > 2$) $\pm$ SD (F) Comparison of ROS production from 1 mg/mL Mal-PEG-TiO_2-UCNs irradiated with NIR or UV light in the presence of tissue phantoms of different thickness, *$P < 0.05$ *versus* ROS production from NIR irradiated Mal-PEG-TiO_2-UCNs. Data are mean ($n = 3$) $\pm$ SD.

greater than -30 mV, which is not considered sufficient to maintain a stable dispersion.[30] Generally, zeta-potential of more than $+30$ mV or less than -30 mV is required to provide enough repulsive forces to counterweigh the van der Waals force of attraction that leads to particle aggregation. Presumably, the low zeta potential (in the range of -25.5 ± 6.8), could be the reason for the observed increase in the hydrodynamic sizes of TiO_2-UCNs in water. On the other hand, in a high ionic strength dispersing media (like PBS and RPMI), the hydrodynamic size of nanoparticles are affected by both the zeta potential and electrical double layer thickness. It is well-known that electrical double layer thickness around the nanoparticles becomes smaller when dispersed in high ionic strength solutions,[29] which correspondingly leads to a weaker electrostatic repulsive force resulting in large sized aggregates. It is worth noting that the zeta-potential of TiO_2-UCNs in PBS is in the range of -24.0 ± 2.3 and that in RPMI without FBS is -9.6 ± 1.3. Thus, both a weak zeta-potential and smaller electrical double layer, could have resulted in the formation of large aggregates in PBS and RPMI. It was then found that binding of serum proteins to the surface of TiO_2-UCNs forming

TABLE 1. Zeta-Potential and Polydispersity Index (PDI) of 100 μg/mL TiO_2-UCN and Mal-PEG-TiO_2-UCNs, Immediately after Dispersing in Various Solutions

	TiO_2-UCN		Mal-PEG-TiO_2-UCN	
	zeta-potential (mV)	PDI	zeta-potential (mV)	PDI
water	-25.5 ± 6.8	0.216 ± 0.012	-15.3 ± 5.3	0.154 ± 0.004
PBS	-24.0 ± 2.3	0.284 ± 0.005	-8.09 ± 0.5	0.183 ± 0.002
RPMI without FBS	-9.6 ± 1.3	0.217 ± 0.002	-8.16 ± 0.3	0.188 ± 0.004
RPMI with 10% FBS	-7.5 ± 0.9	0.204 ± 0.005	-10.4 ± 0.3	0.155 ± 0.008

a "protein corona", helped to maintain dispersion stability.[31] The presence of proteins on the surface of TiO_2-UCNs creates a physical steric barrier, preventing the nanoparticles from approaching one another.[32] Although serum protein binding might momentarily seem to solve the problem of aggregation, it has some serious negative implications as certain components of the protein corona may act as opsonins.[33,34] Opsonization can eventually lead to the recognition and removal of these nanoparticles from circulation by the macrophages of the mononuclear phagocytic system, leading to decreased bioavailability during their application *in vivo*. Thus, it became necessary to surface modify TiO_2-UCNs to improve its dispersion stability, as well as to prevent the attachment of opsonins. PEGylation, constitutes the most efficient and widely used antiopsonization and steric stabilization strategy.[35] Typically, a PEG chain with molecular weight of 2000 Da or greater is required to achieve stealth characteristics,[36] such that it remains invisible to the phagocytic cells. Hence, a maleimide-PEG-silane with a molecular weight of 2000 Da was chosen to surface-modify TiO_2-UCNs. The maleimide group will serve as a reactive functional group for further conjugation of tumor targeting moieties, for targeted delivery of nanoparticles in the future. PEGylation of nanoparticles is known to decreases its surface energy and minimizes the van der Waals force of attraction between the nanoparticles, by increasing the steric distance between them, resulting in stable nanoparticle dispersion.[37] As expected PEGylation of TiO_2-UCNs conferred dispersion stability up to 24 h, with smaller hydrodynamic sizes ($\sim$300 nm), even in the absence of FBS (Figure 2C and Supporting Information, Figure S2E,F). As PEGylation further reduced the negative zeta-potential of TiO_2-UCNs (Table 1), the dispersion stability observed in the case of Mal-PEG-TiO_2-UCNs is assured not by the electrostatic repulsion but by the steric repulsion between the PEG chains. Furthermore, while the polydispersity index (PDI) of TiO_2-UCN was slightly greater than 0.2 in the different solutions except in RPMI with 10% FBS, PDI of Mal-PEG-TiO_2-UCN was less than 0.2, again indicating formation of a stable dispersion (Table 1). To check if PEGylation was successful in reducing protein adsorption, nanoparticles soaked in RPMI with 10% and 100% FBS were centrifuged to separate out the nanoparticles with attached serum proteins. Gel electrophoresis and silver staining revealed that PEGylation significantly reduced, but did not completely exclude, adsorption of serum proteins to the surface of TiO_2-UCNs (Figure 2D). Upon NIR irradiation, both TiO_2-UCNs and Mal-PEG-TiO_2-UCNs generated significant amount of ROS in PBS compared to the corresponding nonirradiated nanoparticles (Figure 2E). In addition to this, we determined the tissue penetration ability of NIR light as well as its ROS production ability following indirect excitation of TiO_2 shell by the upconverted UV light and further compared it with direct excitation of TiO_2 shell with UV light, by utilizing tissue phantoms of varying thickness (ranging from 6 to 10 mm) (Figure 2F). It was found that while there was only about 36% drop in ROS production when irradiated with NIR light in the presence of a 10 mm tissue phantom, there was over 90% drop in ROS generation when irradiated with UV light. Thus, when compared to direct excitation of TiO_2 shell with UV light, indirect excitation with NIR light has the advantage of penetrating thick tissues, which further highlights the suitability of our nanoconstruct in the treatment of solid or deep-seated tumors.

Uptake of Nanoparticles in Macrophage and Cancer Cells. The presence of PEG also reduced the recognition and uptake of nanoparticles by mouse macrophage cells. TiO_2-UCNs were taken up about 4 times more than Mal-PEG-TiO_2-UCNs after 1 h of incubation with macrophage cells (Figure 3A,B).

To optimize the treatment time it is important to determine the time required for maximum number of nanoparticles to bind and be taken up by the target cells. Both TiO_2-UCNs and Mal-PEG-TiO_2-UCNs were incubated with human oral squamous cell carcinoma (OSCC) cells for different time-points, and washed to remove the unbound nanoparticles. Subsequently, the cells were digested and the lysate was quantitatively analyzed for titanium content by inductively coupled plasma atomic emission spectroscopy (ICP-AES). It was found that while PEGylation reduced uptake of nanoparticles by macrophage cells, it significantly enhanced the uptake of nanoparticles into OSCC cells (Figure 3C) compared to TiO_2-UCNs. Moreover, there was significantly greater uptake at 6 h after incubation compared to 3 h incubation. At the end of 6 h incubation, the nanoparticles were

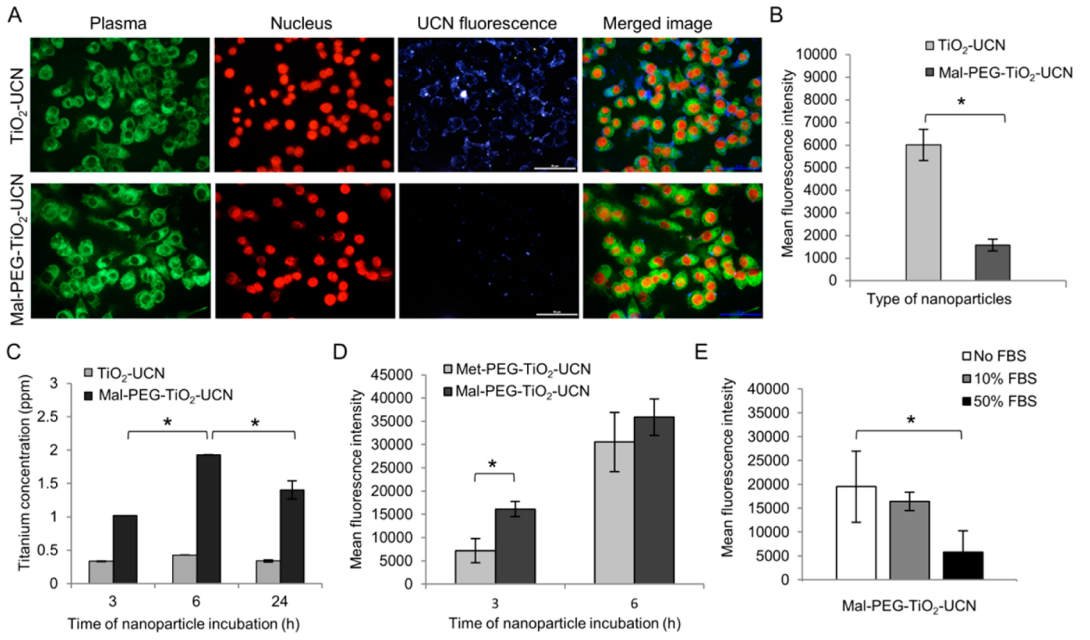

Figure 3. (A) Representative fluorescence microscope images showing blue upconversion fluorescence indicating nanoparticle uptake by macrophages following 1 h incubation with 1 mM of respective nanoparticles; green and red fluorescence indicate cell membrane and nucleus respectively (scale bar: 50 μm). (B) Comparison of fluorescence intensities of nanoparticles at a concentration of 1 mM taken up by macrophages following 1 h incubation; *P = 0.0004. Data are mean fluorescence intensities (n > 3) ± SD. (C) Comparison of titanium content by ICP-AES analysis following uptake of 1 mM TiO_2-UCN or Mal-PEG-TiO_2-UCN in OSCC cells; *P < 0.0001. Data are mean concentration of titanium (n = 2) ± SD. (D) Comparison of fluorescence intensities of 1 mM TiO_2-UCNs surface modified with methoxy-PEG-silane (Met-PEG-TiO_2-UCN) or maleimide-PEG-silane (Mal-PEG-TiO_2-UCN) incubated with OSCC cells; *P < 0.05. Data are mean fluorescence intensities (n > 3) ± SD. (E) Influence of serum proteins in the binding and internalization of 1 mM Mal-PEG-TiO_2-UCNs in OSCC cells following 3 h incubation; *P = 0.0091. Data are mean fluorescence intensities (n > 3) ± SD.

mostly observed in the cytoplasm (Supporting Information, Figure S3). However, following 24 h incubation there was a drop in titanium content compared to the 6 h time point. Thereafter, some of the ingested nanoparticles could have been exocytosed by 24 h.[38,39]

It is often argued that while PEGylation reduced macrophage recognition and uptake, it could in turn lead to reduced cellular uptake, decreasing the therapeutic potential of such nanodelivery systems. However, we observed an increased uptake of Mal-PEG-TiO_2-UCNs by the cancer cells compared to TiO_2-UCNs. As maleimide group rapidly and specifically binds to the thiol group, it is possible that PEG-maleimide-modified nanoparticles could target cell surface thiols, resulting in their enhanced cellular internalization.[40] To further investigate whether the presence of maleimide has indeed favored the binding and uptake of TiO_2-UCNs in cancer cells, we utilized PEG-silane with (maleimide-PEG-silane) and without maleimide group (methoxy-PEG-silane, 2000 Da) to surface modify TiO_2-UCNs, and compare its cell-binding and internalization efficiency in OSCC cell. The results revealed a significant increase in the uptake of Mal-PEG-TiO_2-UCNs into the OSCC cells as early as 3 h (Figure 3D and Supporting Information, Figure S4A), which could be due to the interaction of maleimide group on the nanoparticle with the cell-surface thiols. As a further confirmation, when cell surface thiols were preblocked with N-ethylmaleimide (NEM), we observed 5 fold reduction in the internalization of Mal-PEG-TiO_2-UCNs in cancer cells (Supporting Information, Figure S4B,C). Apparently, if such interactions existed, the maleimide group could also interact with thiols groups on various serum components before reacting with cell surface thiols, leading to suppression of the nanoparticle uptake. Nevertheless, the uptake of Mal-PEG-TiO_2-UCNs was not significantly affected by the presence of 10% FBS compared to the uptake in medium without FBS, but dropped about 4 folds in the presence of 50% FBS (Figure 3E and Supporting Information, Figure S5). Similar results were recently reported using maleimide functionalized liposomes, in which the enhanced uptake in the presence of serum proteins were attributed to the binding of maleimide functionalized nanoparticles to certain serum proteins like albumin, that express reductive cysteine residues and tend to be taken by cells *via* receptor-mediated endocytosis.[41] Although, a higher FBS concentration could be detrimental, 10% FBS was still optimal for the cell internalization process of maleimide functionalized nanoparticles. Apart from the absence of a reactive maleimide group, other possible reasons for the relatively lower uptake of bare TiO_2-UCNs in cancer cells could be large aggregate formation in complex biological environment that might hamper its uptake into the cells.

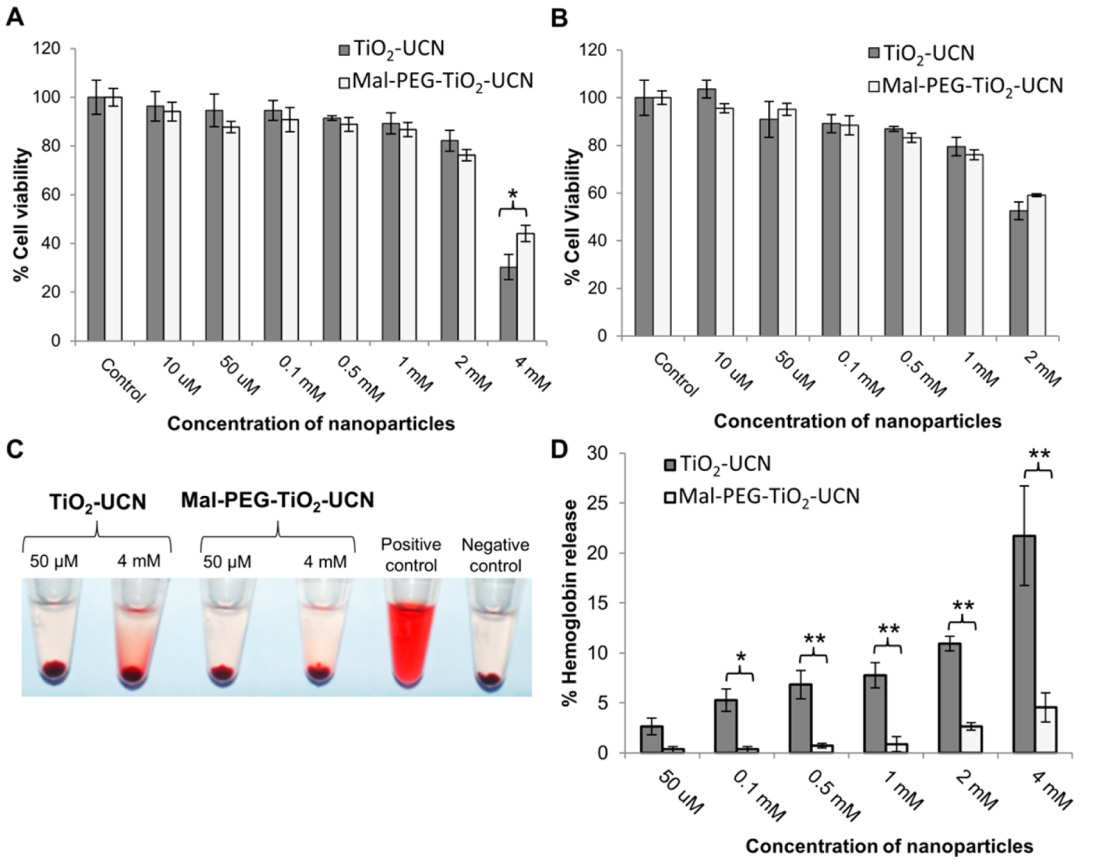

Figure 4. *In vitro* **dark toxicity of nanoparticles incubated with OSCC cells for 6 h using (A) MTT, *P = 0.0082 and (B) trypan blue assay; data are mean (n = 3) ± SD. (C) Photographs of hemolysis of mouse RBCs in the presence of nanoparticles; Triton-X 100 and PBS are used as positive and negative controls, respectively. (D) Rate of hemolysis in RBCs upon 2 h incubation with nanoparticles at incremental concentrations, *P < 0.05, **P < 0.0001; data are expressed as mean ± SD and n = 4.**

Dark-Toxicity of Nanoparticles. We chose human OSCC cells as a model for both *in vitro* and *in vivo* studies as these cells overexpressed epithelial growth factor receptors on its cell surface,[42] which can be utilized to specifically target the developed nanoparticles to these cancer cells in the next phase of our study. It was found that there was no significant difference between cell-viability of untreated OSCC cells and cells treated with TiO_2-UCNs or Mal-PEG-TiO_2-UCN up to a concentration of 1 mM (Figure 4A). At 2 mM, though the cell viability is still above 80%, it is significantly lower than the viability of untreated control cell and drops below 50% at very high concentration of 4 mM. Again, there was no significant difference between the toxicity of unmodified and surface modified TiO_2-UCNs except at high concentration above 2 mM, where the PEGylated TiO_2-UCNs seemed to be significantly less toxic than the unmodified version (P = 0.0082). Although, the cell uptake and dark-toxicity of OSCC cells cannot be compared with normal human fibroblast (NHF) cells, owing to the difference in cell sizes and growth patterns (Supporting Information, Figure S6A), a similar trend in dark-toxicity was also observed when the nanoparticles were incubated with NHF cells (Supporting Information, Figure S6B). As the standard MTS ([3-(4,5-dimethylthiazol-2-yl)-5-(3-carboxymethoxyphenyl)-2-(4-sulfophenyl)-2*H*-tetrazolium) proliferation assay only reflects the mitochondrial enzyme activity, the dark-toxicity of the nanoparticles was also evaluated using the trypan-blue dye exclusion method which is based on the fact that dead cells lose their membrane integrity and becomes permeable to the dye. As expected, this time the viability of OSCC cells dropped slightly more, but again there was no significant difference between cell-viability of untreated OSCC cells and cells treated with TiO_2-UCNs or Mal-PEG-TiO_2-UCN up to a concentration of 1 mM and cell-viability remained above 80% (Figure 4B). Thereafter, it reduced to 60% at a concentration of 2 mM. Hence, for all subsequent *in vitro* work, the maximum concentration of nanoparticles used was fixed at 1 mM.

Hemolysis Assay. The hemocompatibility of the nanoparticles at a concentration range of 50 μM to 4 mM were evaluated with red blood cell (RBC) lysis assay. As shown in Figure 4C,D, both TiO_2-UCNs and Mal-PEG-TiO_2-UCNs displayed a dose-dependent increase in hemoglobin release. However, the RBC lysis caused by TiO_2-UCNs at concentrations greater than 50 μM were significantly greater than Mal-PEG-TiO_2-UCNs. Percent hemolysis levels in 4 mM TiO_2-UCN treated RBCs were 21.7%. On the other hand, the hemoglobin release

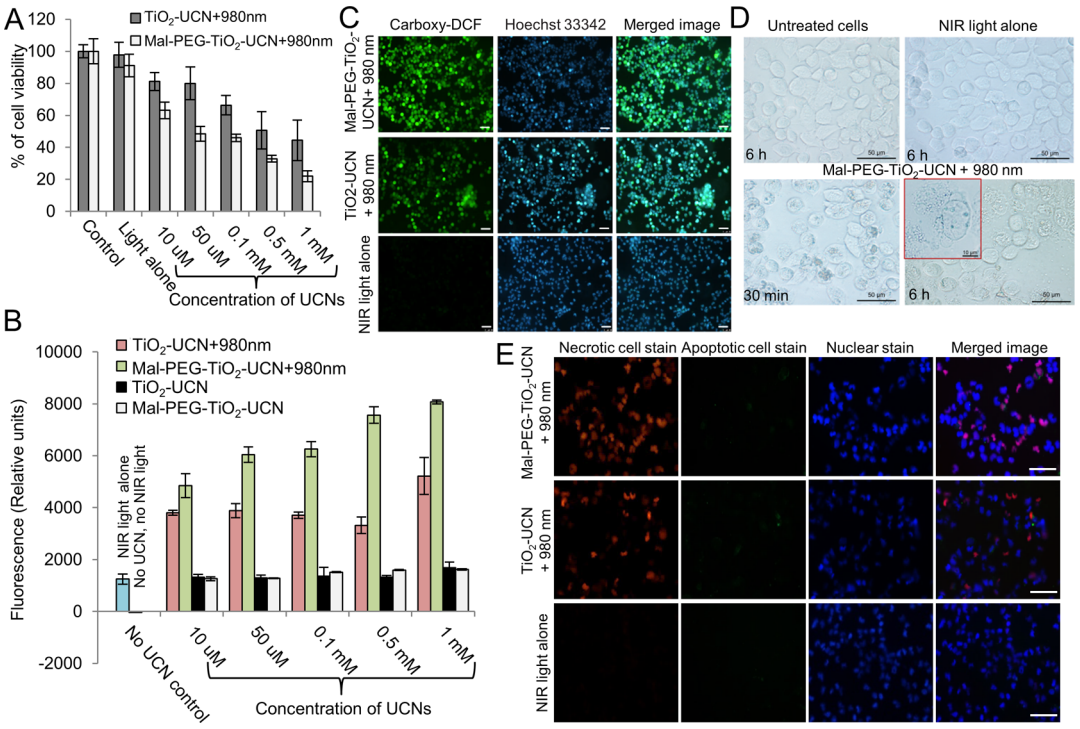

Figure 5. (A) OSCC cell viability 24 h following *in vitro* PDT in the presence of nanoparticles; Control cells are untreated cell assumed to have 100% viability, Light alone control are cells treated with NIR light alone. Data are mean cell viability % ($n = 3$) ± SD. The extent of ROS generated was (B) quantified based on the fluorescence intensity of carboxy-DCF (Data are mean relative fluorescence intensities ($n = 3$) ± SD) and (C) visualized by fluorescence microscopy, images showing green fluorescence indicating positive staining for carboxy-DCF, blue fluorescence indicate nucleus (scale bar: 50 μm). (D) Bright-field live cell images showing mechanism of cell death in OSCC cells counterstained with trypan blue (scale bar: 50 μm), inset shows cells undergoing necrosis (scale bar: 10 μm). (E) Representative fluorescence microscopy images showing mode of cell death after PDT in OSCC treated with 1 mM TiO_2-UCN or Mal-PEG-TiO_2-UCN. Necrotic and apoptotic cells were stained with Ethidium Homodimer III (red fluorescence) and annexin V-FITC (green fluorescence) respectively. Positions of the cells are indicated by nuclear staining with Hoechst 33342 (blue fluorescence), scale bar: 50 μm.

caused by Mal-PEG-TiO_2-UCNs was well below 5% across the range of concentrations investigated. This indicates that PEG modified TiO_2-UCNs exhibit excellent hemocompatibility and is suitable for *in vivo* application.

***In Vitro* PDT and Cell Death.** Before evaluating the efficiency of the synthesized nanoparticles for PDT, it is essential to optimize the PDT parameters like the light dose and time of irradiation such that the NIR light itself does not kill the cells. To achieve this, OSCC cells were subjected to a range of NIR laser dose at 980 nm, to determine a dosage that can be well tolerated by the cell, but is detrimental to the cells in the presence of nanoparticles. Since, here the photocatalyst TiO_2 is excited indirectly by an upconverted UV light (anti-Stokes scheme) and not by direct excitation with UV as in a typical PDT regime, the excitation power density that is required will be relatively higher due to the low efficiency of the upconversion process.[13] It was found that a NIR laser power of 1.2 W under continuous irradiation for 5 min 20 s (at power density of ~2.1 W/cm^2) delivering a light fluence of 675 J/cm^2 was well tolerated by OSCC cells (Supporting Information, Figure S7), with >95% cell viability. At the same time, in the presence of 1 mM Mal-PEG-TiO_2-UCNs, irradiation using this optimized light dose killed about 80% of the cells. Any further decrease in laser power and increase in time of irradiation did not hit such a right balance, leading to the assumption that there exists a minimum threshold excitation power density required by the UCN core, below which it cannot actively upconvert and excite the TiO_2 in the shell to produce sufficient ROS for effective cell killing. On the other hand, a further increase in excitation power density may lead to thermal decline of the cells. Thus, optimization and selection of the best possible light dosage is crucial for the success of PDT. *In vitro* PDT on OSCC cells using the optimized light parameters, showed that Mal-PEG-TiO_2-UCNs produced significantly more cell death (78%) compared to TiO_2-UCNs (56%) at a concentration of 1 mM (Figure 5A). Thus, surface modification of TiO_2-UCNs significantly improved the PDT efficacy of TiO_2-UCNs *in vitro*.

As a further proof that the cell-death is indeed bought about by ROS that is generated by the photoactivation of TiO_2 shell on the UCNs, the ROS generation was quantitatively evaluated within 30 min after irradiation of the cells. At a concentration of 1 mM, the Mal-PEG-TiO_2-UCNs in the presence of 980 nm light produces significant amount of ROS compared to TiO_2-UCNs, resulting in better PDT efficacy probably due to the higher uptake of the nanoparticles by the cancer

cells (Figure 5B). Additionally, it was observed that in the case of Mal-PEG-TiO_2-UCN, there was a considerable dose-dependence in the production of ROS. In contrast, TiO_2-UCNs did not display such a trend. In addition to quantitative analysis, the generated ROS was also imaged using carboxy-2′,7′-dichlorodihydrofluorescein (carboxy-H_2DCHF), a fluorogenic marker for ROS. Here, the nonfluorescent carboxy-2′,7′-dichlorodihydrofluorescein (carboxy-H_2DCHF) is oxidized to fluorescent carboxy-DCF (bright green fluorescence) in the presence of ROS. As a result of the photocatalytic damage induced by modified and unmodified TiO_2-UCNs upon NIR irradiation, there was a significant number of cells exhibiting bright green fluorescence representing oxidative stress in the presence of ROS (Figure 5C). Again, the fluorescence from the cells treated with Mal-PEG-TiO_2-UCNs was visibly much stronger than that treated with the unmodified version, which correlated with the cell-viability results following *in vitro* PDT.

Furthermore, it was found that when Mal-PEG-TiO_2-UCNs were incubated for a shorter duration of 1 h, the particles were mostly seen attaching to the cell membrane, with very minimal uptake of the particles into the cells (Supporting Information, Figure S8). However, after 6 h of incubation the particles were mostly seen inside the cell, predominantly in the cytoplasm. Although, a longer incubation time was required for the uptake of nanoparticles within the cytoplasm, we expected that a short drug-light interval could likely be sufficient to produce enough cell kill by disruption of the membrane integrity by the ROS. On comparing the cell-viability, it was observed that there was about 50% cell death following PDT after a mere 1 h incubation of Mal-PEG-TiO_2-UCN. Nevertheless, cell death was more pronounced (>70%) following PDT after 6 h incubation. This observation is consistent with our *in vitro* nanoparticle uptake data, that there is a higher uptake of nanoparticles after a 6 h incubation period, due to which there was a greater cell-kill following PDT. But the significance of this observation is that the mere attachment of the nanoparticles to the cell-membrane itself could kill a significant number of cells. In an *in vivo* setting, this could imply that it might not be essential for the nanoparticles to enter the cells to achieve a reasonable amount of tumor cell kill following PDT. However, for a more rounded and effective PDT outcome perhaps the uptake of the nanoparticles into the cell will be desirable as an incomplete treatment would often lead to a rapid relapse of the tumor.

Having established that ROS is the major causative agent for cell death following NIR mediated photocatalytic activation of TiO_2, the next step was to determine the mechanism of cell death. PDT is known to induce cell-death by apoptosis, necrosis or autophagy depending on the cell type, the nature and localization of the PSs and the light dose.[43,44] When untreated OSCC cells and cells irradiated with NIR light alone were stained with trypan blue, very few cells seemed to take up the blue dye within 30 min of light irradiation (Figure 5D). However, when the cells were incubated with Mal-PEG-TiO_2-UCNs for 6 h and then irradiated with NIR light, majority of the cells stained blue within 30 min of treatment, indicating loss of membrane integrity although the cells appeared to maintain its shape. Six hours after NIR light irradiation, there was cell membrane blebbing and complete rupture of cell membrane suggesting severe cellular insult *via* necrotic pathway of cell death. To further confirm this, the cells were stained 30 min after treatment with FITC-Annexin V, Ethidium Homodimer III and Hoechst 33342 that stains apoptotic cells green, necrotic cells red and nuclei blue, respectively. It was found that majority of the cells incubated with Mal-PEG-TiO_2-UCNs and TiO_2-UCNs underwent necrosis, staining red and blue (Figure 5E).

***In Vivo* Imaging and PDT Treatment Efficacy.** In order to determine the time of homogeneous distribution of UCNs in the tumor following intratumoral injection of Mal-PEG-TiO_2-UCNs, animals were imaged by an *in vivo* optical imaging system using an external 980 nm laser excitation source. Bright upconversion luminescence (UCL) emission was captured using an 810 nm emission filter, 30 min and 6 h after administration (Figure 6A). However, the UCL from the tumor at 6 h was better distributed across the tumor compared to that at 30 min.

To better understand the distribution of particles within the tumor, we studied the UCL emission from the tumor tissue excised 4 h after intratumoral administration of the nanoparticles. It was found that Mal-PEG-TiO_2-UCNs distributed well throughout the tissue at a greater extend compared to unmodified TiO_2-UCNs (Figure 6B). This could perhaps be due to the smaller size of the PEGylated TiO_2-UCNs that favored the efficient diffusion and distribution of the nanoparticles into the deeper layers, as well as the presence of the reactive maleimide group which could have led to its internalization into the tumor cells. Following NIR irradiation of the tumor, an eschar tissue was formed within 48 h in animals treated with Mal-PEG-TiO_2-UCNs (Figure 6D). However, in animals irradiated with NIR-light alone no skin discolouration was observed (Figure 6C). Evan's blue vital staining was done to compare the effect of NIR light alone and NIR light irradiation following intratumoral administration of Mal-PEG-TiO_2-UCN. It was found that the NIR light alone did not cause any tumor tissue necrosis where as in tumors that were irradiated 4 h after intratumoral administration of nanoparticles, a clear unstained necrotic area was observed 48 h after PDT (Figure 6C,D). This confirmed that a 4 h drug-light interval allowed sufficient distribution of nanoparticles within the tumor from the site of injection. H&E staining of tumor slices from animals that were treated with Mal-PEG-TiO_2-UCN + 980 nm, revealed severe destruction of tumor cells in

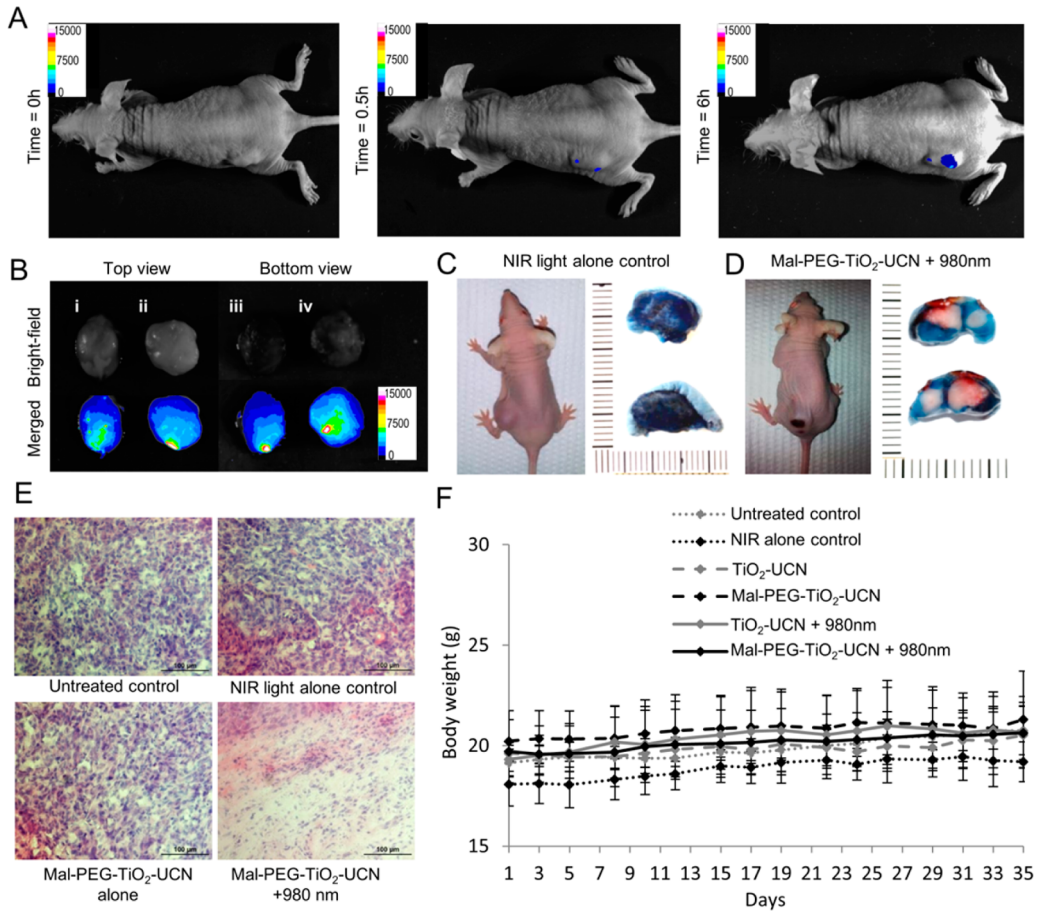

Figure 6. (A) *In vivo* imaging of upconversion luminescence in live mouse upon excitation with 980 nm laser using a 810 nm emission filter before (time = 0 h) as well as 0.5 h and 6 h after intratumoral administration of 0.1 mg of Mal-PEG-TiO_2-UCN. (B) Representative UCL images from excised tumor tissues (from the top and bottom) 4 h after intratumoral administration of 0.1 mg TiO_2-UCNs (i) and (iii) and Mal-PEG-TiO_2-UCNs (ii) and (iv). Representative images of mouse 48 h post-PDT treated with (C) NIR light alone (1000 J/cm^2) (D) intratumorally injected with Mal-PEG-TiO_2-UCN + NIR light (1000 J/cm^2) and sections of tumor tissue excised from the respective mouse 6 h after intraperitoneal injection of Evan's blue vital stain. (E) H&E stained sections of tumor tissue excised from untreated control, NIR alone control, Mal-PEG-TiO_2-UCN alone and Mal-PEG-TiO_2-UCN + NIR light treated mouse (48 h after treatment), Scale bar = 100 μm. (F) Change in body weight of mice in different groups following treatment for up to 35 days.

marked contrast to the tumor slices from control animals (untreated control, NIR light alone and Mal-PEG-TiO_2-UCN alone) (Figure 6E). As the body weight of the animal reflects its overall health condition, the weight of the animals in different groups were measured and plotted as a function of time for up to 35 days. There was no significant decrease in body weight in any of the animals (Figure 6F). Our preliminary findings reveal that PDT treatment using TiO_2-UCNs could possibly be a safe therapeutic procedure.

The PDT treatment efficacy of the developed nanoconstruct was then explored by recording the tumor volume and survival rates of the animals. The untreated control animals and animals that were treated with NIR light alone, TiO_2-UCN alone or Mal-PEG-TiO_2-UCN alone with no light irradiation did not show any therapeutic effect (Figure 7A,B and C). For animals with tumors that were intratumorally injected with TiO_2-UCNs or Mal-PEG-TiO_2-UCNs and exposed to NIR light, there was significant delay in tumor growth compared to the control groups. Although there was a clear reduction in the tumor size in both TiO_2-UCN and Mal-PEG-TiO_2-UCN injected groups after NIR-PDT with in the first 5 days, a complete tumor inhibition was not observed in these groups with a single PDT regimen. Perhaps a second round of PDT about 2 weeks after the first dose, when the residual tumor starts to regrow, could result in a better control of tumor growth and prevent tumor relapse. Survival rates of mice in untreated control, NIR alone control, TiO_2-UCN alone and Mal-PEG-TiO_2-UCN alone treated groups reduced to 40% at day 29, 31, 33, and 36 respectively (Figure 7D). On the other hand, there was a 40% reduction in survival rate of mice treated with TiO_2-UCNs + 980 nm by day 60, whereas no mice died in the group that was treated with Mal-PEG-TiO_2-UCN + 980 nm. Systemic delivery of the nanoparticles require optimization of various factors, such as the concentration of the nanoparticles, drug-light interval and in terms of the nanomaterial, better surface functionalization/bioconjugation strategies might be necessary to allow targeted delivery of the nanoconstructs to the tumor, which will be the focus of our future studies.

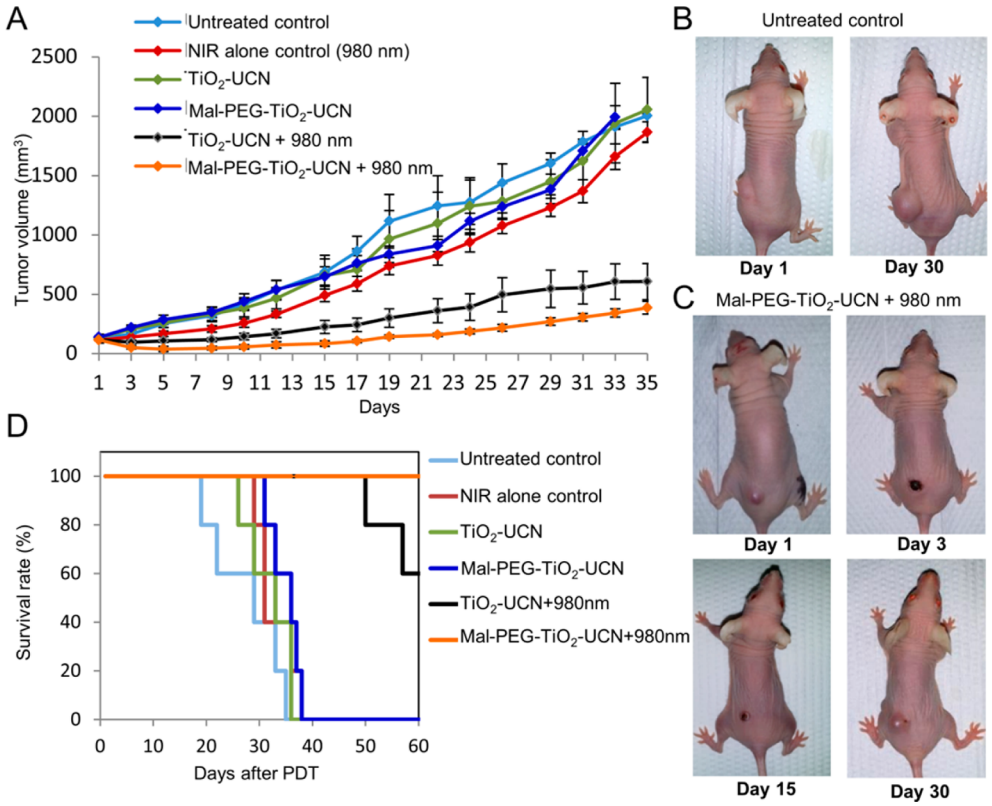

Figure 7. (A) *In vivo* OSCC tumor growth up to 35 days on different groups of mice after various treatments indicated, $n = 5$ per group. Error bars represent standard error of the mean (SEM). Representative images of animals with tumors that were (B) not treated (untreated control animals) and (C) intratumorally injected with 0.1 mg of Mal-PEG-TiO_2-UCN and irradiated with 980 nm light, at designated time-points. (D) Survival rates of mice in different treatment groups within 60 days.

As a matter of fact, the PDT outcome *in vivo* ultimately depends on various factors such as the location, type, aggressiveness and oxygenation of the tumor, the type, concentration and localization of the photosensitizing molecule within the tumor microenvironment at the time of irradiation, the drug-light interval, and the light parameters such as the total light dose, light fluence rate and time of irradiation.[2,45−47] Hence, it is critical to customize the treatment parameters and regimen, depending on these factors for an optimal PDT outcome.

CONCLUSION

Controlling the amount of PS loaded in UCN constructs and achieving stable loading of sufficient amount of PS has been one of the major bottlenecks in the design of UCN based PDT nanoplatforms impeding its translation to even distantly comparable advances in the clinics. We adopted a different approach of surface coating photocatalyst TiO_2 on UCN core to achieve small, uniform sized nanoconstructs, with stable loading of the PS. Our method ensures the formation of a well-defined core−shell structured nanoconstruct in which a single monodisperse UCN core is surrounded by a thin layer of TiO_2, the amount of which can be precisely controlled. Our *in vitro* and *in vivo* results clearly indicate the potential application of this biocompatible nanoconstruct in NIR-triggered deep-tissue PDT. On comparing with previous reports on direct excitation of TiO_2 nanoparticles with UV light that has little or no tissue penetrating abilities, our method of indirectly exciting TiO_2 shell *via* NIR light has the potential to significantly improve the treatment, transforming it into a "minimally invasive" procedure from being an "invasive" technique. Our proof-of-concept demonstration strongly motivates further development and testing of *in vivo* toxicity and biodistribution of these nanoconstructs following systemic administration, as well as fine-tuning of the treatment parameters, that are under way. Carrying out these future studies will undoubtedly improve the performance and therapeutic efficacy of this technology, which may indeed encourage its application in clinics in the near future.

EXPERIMENTAL METHODS

Synthesis of $NaYF_4$:Yb,Tm @SiO_2 Upconversion Nanoparticles. The $NaYF_4$:Yb,Tm UCN core was synthesized as previously reported.[48] Briefly, 0.8 mmol YCl_3, 0.2 mmol $YbCl_3$ and 0.005 mmol $TmCl_3$ were mixed with 6 mL of oleic acid and 15 mL of octadecene in a 50 mL flask and heated to 160 °C to form a homogeneous solution. After cooling it down to RT,

10 mL of methanol solution containing 2.5 mmol NaOH and 4 mmol NH_4F was slowly added into the flask and stirred for 30 min. The solution was subsequently heated to remove methanol, degassed at 100 °C for 10 min, followed by heating to 300 °C and was finally maintained under Argon protection for 1 h. When the solution cooled down to RT, nanocrystals were precipitated from the solution with ethanol, and washed three times with 1:1 ethanol/water (v/v). Subsequent silica coating on the UCN core ($NaYF_4$:Yb,Tm @SiO_2) was done following previous published methods.[49] Briefly, 0.1 mL of CO-520 and 6 mL of cyclohexane were mixed with 4 mL of 0.01 M $NaYF_4$ nanosphere solution in cyclohexane and stirred for 10 min. 0.4 mL of CO-520 and 0.08 mL of ammonia (30 wt %) were then added and the container was sealed and sonicated for 20 min until a transparent emulsion was formed. 0.04 mL of TEOS was then added and the solution was rotated for 2 days at a speed of 600 rpm. $NaYF_4$:Yb,Tm @SiO_2 nanospheres were then precipitated by adding acetone, and the nanospheres were washed twice with 1:1 ethanol/water (v/v) and then stored in water.

Coating of TiO_2 on $NaYF_4$:Yb,Tm @SiO_2. Amino groups were first modified on the silica surface by grafting (3-aminopropyl)-trimethoxysilane (APS) on the $NaYF_4$:Yb,Tm@SiO_2 by adding 0.008 mmol APS into the solution containing 0.02 mmol $NaYF_4$:Yb,Tm@SiO_2 during the silica coating procedure. In a typical synthesis, 0.02 mmol APS grafted $NaYF_4$:Yb,Tm @SiO_2 was dispersed in 10 mL of isopropanol, 0.3 mL of ammonia (28 wt %) and 2.5 mL of water. Then, 2 mL of 0.001 M titanium diisopropoxide bis(acetylacetonate) solution in isopropanol was slowly added and stirred for 24 h at RT. Amorphous TiO_2-UCNs were then collected by centrifugation and washed twice with isopropanol. To achieve a crystallized TiO_2 shell, the TiO_2-UCNs were treated with anhydrous ethanol in a sealed autoclave at 180 °C for 24 h under an air atmosphere.

Surface Modification of TiO_2-UCNs with Maleimide-PEG-Silane. 4 mg of maleimide-PEG-silane (Nanocs Inc., New York, USA) was dissolved in 4 mL of water, to which 4 mg of TiO_2-UCN dispersed in 4 mL of ethanol was added. Subsequently, 10 μL of TEOS was added and the solution was stirred at RT for 30 min. At the end of stirring, 150 μL of ammonia (28 wt %) was added dropwise to the solution and stirred for another 3 h at RT. Mal-PEG-TiO_2-UCNs were then collected by centrifuging solution at 8000 rpm for 10 min at 10 °C, washed twice with ethanol and then stored at 4 °C. For comparison, PEG-silane without maleimide group (methoxy-PEG-silane 2000 Da, Nanocs Inc., New York, USA) was also used to surface modify TiO_2-UCNs using the same protocol.

Characterization of Synthesized Nanoparticles. Size and morphology of the synthesized nanoparticles were characterized using a JEOL 2010 TEM operating at an acceleration voltage of 200 kV. Fluorescence spectra was recorded on a SpectroPro 2150i spectrophotometer (Roper Scientific Acton Research, MA) equipped with a 1200 g/mm grating and 980 nm VA-II diode pumped solid-state (DPSS) laser. FT-IR spectra were recorded on a Shimadzu IRPrestige-21 model spectrometer (Shimadzu Corporation, Kyoto, Japan). DLS was conducted with the Zetasizer (Nano ZS, Malvern Instruments Ltd., UK) to measure the hydrodynamic diameter, PDI and zeta-potential. Nanoparticles at a concentration of 1 mg/mL in deionized water were sonicated for 20 min before further diluting (100 μg/mL) it in water, PBS, RPMI and RPMI with 10% FBS to determine the average aggregate size with time.

Measurement of ROS Production in Solution. To measure the ROS generation ability of the unmodified and modified TiO_2-UCNs, aminophenyl fluorescein (APF) (Molecular Probes, Inc., USA) was used as an indicator. UCNs at a concentration of 1 mg/mL in PBS were sonicated for 20 min and APF dye at a final concentration of 10 uM was added to the UCN suspension. The fluorescence of suspension was measured before irradiation at 515 nm by a UV−vis spectrophotometer (Photonitech, Singapore) under excitation at 490 nm, which is denoted as fluorescence intensity at time 0 h (t = 0). The suspension was then irradiated using 980 nm NIR light at a power of 1.2 W for up to 60 min, measuring the fluorescence at every 20 min of irradiation. As the amount of generated ROS is proportional to the fluorescence intensity of APF, the fluorescence intensity is plotted as a function of exposure time.

To demonstrate the tissue penetration abilities, the same experiment was performed by placing tissue phantoms of varying thickness (6−10 mm), in the path of the incident NIR or UV light. Briefly, the tissue phantoms were prepared using 0.5% (w/v) ultrapure agarose, (Invitrogen), 1% (v/v) of intralipid-10% (Kabivitrum Inc.,) as the scatterer and 0.1% (v/v) Nigrosin, as the absorber. The tissue penetration and ROS generation abilities of NIR and UV light was expressed as percentage drop in ROS generation from 1 mg/mL Mal-PEG-TiO_2-UCNs following irradiation in the presence of tissue phantoms as compared to direct irradiation of the sample with NIR or UV light without the tissue phantom.

Gel Electrophoresis and Silver Staining. The nanoparticles (TiO_2-UCNs and Mal-PEG-TiO_2-UCNs) at a concentration of 1 mg/mL were treated in RPMI with 10% FBS or 100% FBS for 24 h. The suspension was then carefully layered over 10% glycerol and centrifuged at 15 000 rpm for 15 min. The pellet was collected and resuspended in 200 μL of deionized water. Equal volume of this sample was treated with 2× Laemmli sample buffer (Bio-Rad, USA) and heated for 5 min at 95 °C to reduce the disulfide bonds. The samples were then loaded on a 5% Sodium dodecyl sulfate-polyacrylamide gel electrophoresis (SDS-PAGE) gel to separate SDS-denatured proteins at 120 V for 2.5 h. The protein bands were silver stained using the Pierce Silver Stain Kit (Thermo Scientific, USA), following manufacturer's instructions.

Cell Lines. OSCC (CAL-27), mouse leukemic monocyte macrophage cell line (RAW 264.7) and NHF cells (IMR-90) were purchased from American Type Culture Collection (ATCC, USA). The cells were cultured in RPMI-1640 medium (OSCC cells) and Dulbecco's modified Eagle's medium (DMEM) (Macrophages and NHF cells). The media were supplemented with 10% FBS and 1% penicillin-streptomycin. Cells were maintained at 37 °C in a humidified atmosphere containing 5% CO_2.

***In Vitro* Macrophage Uptake Assay.** RAW 264.7 mouse macrophages were seeded in 8-well chambered slide at a cell density of 25 × 10^3 cells per well and incubated overnight to allow the cells to adhere to the floor of the wells. The medium in the wells were replaced with a nanoparticle suspension (TiO_2-UCN or Mal-PEG-TiO_2-UCN) at a concentration of 1 mM (270 μg/mL) in DMEM supplemented with 10% FBS and incubated for 1 h at 37 °C. The macrophage cells were then rinsed thrice with 1 × PBS to wash away the excess noningested nanoparticles and fixed in ice-cold methanol for 10 min. The plasma membrane was stained with Wheat Germ Agglutinin, Alexa Fluor 488 Conjugate (Molecular Probes, Inc., USA) at a concentration of 5 μg/mL for 10 min. The nucleus was further counterstained with propidium iodide (Molecular Probes, Inc., USA) at a concentration of 500 nM for 5 min. The cell were gently washed thrice with PBS and mounted using Vectashield mounting medium (Vector Laboratories, CA, USA). The uptake of unmodified and modified TiO_2-UCNs by the macrophages was imaged using an upright Nikon 80i Fluorescence Microscope (Nikon, Tokyo, Japan) equipped with a 980 nm Laser Wide-field Fluorescence add-on (EINST Technology Pte Ltd., Singapore) using a 20X objective (200× magnification). The plasma membrane and nuclei of the cells were visualized under excitation with Hg arc lamp and a standard FITC and TRITC filter set, respectively. The uptake of unmodified and modified TiO_2-UCNs by macrophages was also compared by measuring the total fluorescence intensities of UCNs using the ImageJ 1.47v software (National Institute of Health, USA).

***In Vitro* Dark-Toxicity Measurement.** OSCC and NHF cells were seeded at a cell density of 8 × 10^3 per well in a 96-well plate and incubated overnight to allow it to adhere to the bottom of the plate. The nanoparticles (TiO_2-UCNs or Mal-PEG-TiO_2-UCNs) were prepared at a concentration of 1 mg/mL in sterile PBS, sonicated for 20 min and then diluted in RPMI with 10% FBS at varying concentrations ranging from 10 μM (2.7 μg/mL) to 4 mM (1.08 mg/mL) before adding to the cells. Cells were further incubated for 6 h at 37 °C after which they were gently washed 3 times with 1 X PBS to remove the nanoparticles and replaced with fresh culture media. Following 24 h incubation at 37 °C, the number of viable cells was determined by MTS assay using CellTiter 96 Aqueous One Solution Cell Proliferation Assay (Promega, Madison, WI, USA) kit as per manufacturer's

instructions. The percent cell viability values are reported relative to those of untreated control cells.

For trypan blue staining, 8×10^4 OSCC cells were seeded in a 12 well plate and treated with nanoparticles as mentioned above. The cells in each of the wells were harvested and collected by centrifugation at 1200 rpm for 5 min. The cells were then stained with 0.4% trypan blue solution in PBS for 5 min before counting using a dual-chamber hemocytometer and a light microscope. Total number of cells and dead (blue colored) cells were recorded, and the means of three independent cell counts were pooled for analysis. The percentage of viable cells was determined by according to the following formula. Percent of viable cells =100[(total number of cells − number of dead cells)/(average number of cells in the control untreated well)].

Hemolysis Assay. Female balb/c nude mice, 6−8 weeks of age, weighing an average of 17 g were obtained from BioLasco, Taiwan. Fresh blood (≈1 mL) was obtained from mice *via* cardiac puncture. All procedures carried out in this study were approved by the Institutional Animal Care and Use Committee (IACUC), SingHealth, Singapore and were conducted in accordance with international standards. Red blood cells (RBCs) were separated from plasma by centrifuging at 1500 rpm for 15 min at 4 °C. The isolated RBCs were further washed three times with sterile PBS by centrifugation until the supernatant was clear, and resuspended in 2 mL of PBS. Then 100 μL of the nanoparticle (both TiO_2-UCN and Mal-PEG-TiO_2-UCN) suspension in PBS at concentrations ranging from 50 μM to 4 mM were added to 100 μL of the RBCs suspension. Following a 2 h at 37 °C under constant shaking, the suspensions were centrifuged at 1500 rpm for 15 min. Subsequently, 100 μL of supernatant from each centrifuge tube was used to analyze hemoglobin release by microplate reader at the wavelength of 576 nm. Control experiments were performed under the same experimental conditions, where 100 μL of the RBCs suspension was added to 100 μL of PBS as a negative control and to 100 μL of 0.5% Triton X-100 as a positive control. The percentage hemolysis was calculated using the following equation:

$$\text{Hemolysis}\ (\%) = (\text{OD576 sample} - \text{OD576 negative control}) / (\text{OD576 positive control} - \text{OD576 negative control}) \times 100\%$$

***In Vitro* Uptake of Nanoparticles.** OSCC cells were seeded in a 145 cm^2 cell-culture dish at a density of 3×10^6 cells per dish and incubated at 37 °C overnight. Cells were treated with UCNs at a concentration of 1 mM for 3, 6, or 24 h, following which the culture medium containing noninternalized nanoparticles were discarded, and the cells were washed three times with phosphate-buffered saline. The cells were then harvested, and the intracellular uptake of nanoparticles was determined by measuring the titanium, yttrium and ytterbium content using ICP-AES.

For imaging uptake of nanoparticles, OSCC and NHF cells were seeded in 8 well chambered slide and incubated overnight; following which the cells were treated with Mal-PEG-TiO_2-UCNs at a concentration of 1 mM for 6 h. The cells were then fixed with ice-cold methanol for 10 min; plasma membrane and nuclei were stained with Wheat Germ Agglutinin, Alexa Fluor 488 Conjugate and propidium iodide, washed, coverslipped and imaged using a Nikon 80i Fluorescence Microscope (Nikon, Tokyo, Japan) using a 40× objective (400× magnification) under excitation with Hg arc lamp and a standard FITC, TRITC and DAPI filter set. Furthermore, the uptake of Mal-PEG-TiO_2-UCNs and Met-PEG-TiO_2-UCNs in OSCC cells at various incubation conditions was quantified by measuring the total fluorescence intensities of UCNs using the ImageJ 1.47v software (National Institute of Health, USA). To check the influence of NEM on the cellular uptake of Mal-PEG-TiO_2-UCNs, OSCC cells were preblocked with 1 nM NEM in serum free RPMI for 15 min, followed by 6 h incubation with 1 mM Mal-PEG-TiO_2-UCNs.

***In Vitro* PDT.** OSCC cells were seeded into 96-well cell culture plate at a cell density of 8×10^3 cells per well. Following overnight incubation at 37 °C, the cells were treated with various concentrations of unmodified and surface modified TiO_2-UCNs ranging from 10 μM to 1 mM for 6 h. The medium containing noninternalized nanoparticles were removed and the cells were washed thrice with PBS, and replaced with fresh culture medium. The cells were then irradiated using 980 nm NIR light at a power of 1.2 W for 5 min 20 s delivering a total fluence of 675 J/cm^2.The cells were incubated for additional 24 h before percentage of cell viability relative to the control untreated cells was determined using CellTiter 96 AQueous One Solution Cell Proliferation Assay (Promega, Madison, WI, USA) as per manufacturer's instructions.

Measurement of ROS Production *In Vitro*. The amount of ROS generated following *in vitro* PDT using TiO_2-UCNs or Mal-PEG-TiO_2-UCNs was measured using OxiSelect *in vitro* ROS/RNS Assay Kit (CellBiolabs, Inc. USA) following the manufacturer's instruction. Briefly, OSCC cells were seeded into 96-well cell culture plate at a cell density of 8×10^3 cells per well. Following overnight incubation at 37 °C, the cells were then treated with TiO_2-UCNs or Mal-PEG-TiO_2-UCNs for 6 h, following which the medium was removed and replaced with 100 μL of the nonfluorescent 2′,7′-dichlorofluorescein (DCFH) for 1 h. The cells were then gently washed thrice with 1X PBS and fresh medium was added to each well followed by 980 nm NIR light irradiation using same light dose as mentioned above. The ROS generated in the cells was determined fluorometrically by measuring the amount of 2′, 7′-dichlorodihydrofluorescein (DCF) produced and comparing it with predetermined DCF standard curve.

Assessment of Mode of Cell-Death. To study the mode of cell death following *in vitro* PDT, OSCC cells were lightly counterstained with 0.1% trypan blue in PBS for 5 min at different time intervals after treatment (30 min and 6 h). The cells were then gently washed once with 1 X PBS and coverslipped with HBSS and immediately visualized using a bright field microscope fitted with a Nikon DS-Ri1 camera.

To further assess the mechanism of cell death following PDT, Promokine apoptotic/necrotic/healthy cells detection kit (PromoCell GmbH, Germany) was used according to manufacturer's instruction. Briefly, OSCC cells adhering to the bottom of 8-well chambered slide were subjected to PDT following which the slides were returned to 37 °C incubator for the PDT effect to take place. The cells were then washed twice with 1× binding buffer and stained with staining solution containing 5 μL of FITC-Annexin V, 5 μL of Ethidium Homodimer III and 5 μL of Hoechst 33342 in 100 μL 1× binding buffer for 15 min at RT. The cells were further washed twice with 1× binding buffer and coverslipped with 1X binding buffer. Images were acquired on a Nikon 80i Fluorescence Microscope (Nikon, Tokyo, Japan) using a 20× objective (200× magnification) under excitation with Hg arc lamp and a standard FITC, TRITC and DAPI filter set.

***In Vivo* Imaging.** *In vivo* imaging following intratumoral administration of 0.1 mg of Mal-PEG-TiO_2-UCNs was performed using the uFluor-980 small animal fluorescence upconversion imaging system (Einst Technology Pte Ltd., Singapore). Briefly, 0.1 mg of Mal-PEG-TiO_2-UCN in 40 μL saline was intratumorally injected at 2 or more sites. Imaging was performed before as well as 30 min and 6 h after administration of particles under 980 nm laser excitation delivering a fluence rate equivalent to 250 mW/cm^2. Similarly, UCL images from tumor tissues excised from mouse at 4 h after injection of 0.1 mg of TiO_2-UCNs or Mal-PEG-TiO_2-UCNs, were also captured using 810 nm emission filter.

***In Vivo* PDT Treatment.** Animals were assigned to six different groups: (i) control (untreated tumor), (ii) NIR-light alone control (1000 J/cm^2), (iii) TiO_2-UCN alone (0.65 mg/tumor), (iv) Mal-PEG-TiO_2-UCN alone (0.65 mg/tumor), (v) TiO_2-UCN (0.1 mg/tumor) + PDT (1000 J/cm^2), and (vi) Mal-PEG-TiO_2-UCN (0.1 mg/tumor) + PDT (1000 J/cm^2), and each group comprised of 5 animals. Tumor volume was measured when tumors reached a size of 120 mm^3. For group (ii), tumors were irradiated with 980 nm NIR light at a power of 500 mW for 33 min 20 s. For groups (iii) and (iv), tumors were intratumorally injected with 40 μL of respective UCNs. For groups (v) and (vi), 4 h after intratumoral administration of 40 μL of respective UCNs, the tumors were irradiated with NIR light. For all groups, tumor volume was measured on at least 3 alternate days a week, for up to 35 days. The tumor volume was calculated using the following formula: Volume = (π/6 × d1 × d2 × d3), where d1, d2 and d3 are tumor dimensions in 3 orthogonal directions. For Evan's blue staining,

400 μL of 1% Evan's blue dye in saline was injected intraperitoneally into the animals 48 h after treatment and 6 h later the animals were sacrificed to excise the tumors. 2−3 mm thick cross-section slices of tumors were cut and imaged under a stereoscopic microscope (Stemi 2000C, Zeiss, Germany). For H&E staining, tumors were excised 48 h after treatment and snap-frozen in liquid nitrogen. Serial 8 μm thick cryosections were fixed in acetone, stained with H&E and imaged by a Nikon 80i digital microscope (Nikon, Tokyo, Japan) using a 20× objective (200× magnification)

Statistical Analysis. In all figures, data points represent mean ± standard deviation (SD). Statistical analyses were performed using the GraphPad Prism version 6.0 software (GraphPad Software, San Diego California USA). Differences in means were compared with two-tailed unpaired Student's *t* -test or using two-way ANOVA followed by Bonferroni's posthoc test. *P* values less than 0.05 ($P < 0.05$) were considered significant.

Conflict of Interest: The authors declare no competing financial interest.

Acknowledgment. The authors would like to acknowledge the funding support from Agency for Science, Technology and Research (A*STAR) Biomedical Engineering Programme: Grants R-397-000-128-305 (National Univeristy of Singapore) and BMRNI11133 (National Cancer Centre Singapore). Lucky S. S. is a recipient of NGS scholarship from NUS graduate school (NGS) for Integrative Sciences and Engineering, National University of Singapore. The authors would also like to thank the members of Tan Chin Tuan Laboratory of Optical Imaging and Photodynamic Therapy, National Cancer Centre Singapore, for providing their research facility for conducting the experiments.

Supporting Information Available: TEM images of $NaYF_4$:Yb, Tm core, $NaYF_4$:Yb,Tm@SiO_2 and TiO_2-UCN before annealing, fluorescence emission spectra of TiO_2-UCNs under *in vitro* and *in vivo* excitation power densities, PDI and DLS measurements of TiO_2-UCNs in various solutions, photographs of nanoparticles suspended in PBS, confocal fluorescence microscopic image showing localization of Mal-PEG-TiO_2-UCNs in cells, fluorescence images comparing cellular uptake of Met-PEG-TiO_2-UCNs and Mal-PEG-TiO_2-UCNs, fluorescence images comparing cellular uptake of nanoparticles in OSCC and NHF cells, dark-toxicity of NHF cells, optimization of NIR laser dose for *in vitro* PDT and comparison of cell uptake, viability and *in vitro* ROS generation ability of Mal-PEG-TiO_2-UCN incubated with cells for different periods. This material is available free of charge *via* the Internet at http://pubs.acs.org.

REFERENCES AND NOTES

1. Konan, Y. N.; Gurny, R.; Allemann, E. State of the Art in the Delivery of Photosensitizers for Photodynamic Therapy. *J. Photochem. Photobiol., B* **2002**, *66*, 89–106.
2. Dougherty, T. J.; Gomer, C. J.; Henderson, B. W.; Jori, G.; Kessel, D.; Korbelik, M.; Moan, J.; Peng, Q. Photodynamic Therapy. *J. Natl. Cancer Inst.* **1998**, *90*, 889–905.
3. Nowis, D.; Makowski, M.; Stoklosa, T.; Legat, M.; Issat, T.; Golab, J. Direct Tumor Damage Mechanisms of Photodynamic Therapy. *Acta. Biochim. Polym.* **2005**, *52*, 339–352.
4. Castano, A. P.; Mroz, P.; Hamblin, M. R. Photodynamic Therapy and Anti-Tumour Immunity. *Nat. Rev. Cancer* **2006**, *6*, 535–545.
5. Thong, P. S.; Ong, K. W.; Goh, N. S.; Kho, K. W.; Manivasager, V.; Bhuvaneswari, R.; Olivo, M.; Soo, K. C. Photodynamic-Therapy-Activated Immune Response against Distant Untreated Tumours in Recurrent Angiosarcoma. *Lancet Oncol.* **2007**, *8*, 950–952.
6. Thong, P. S.; Olivo, M.; Kho, K. W.; Bhuvaneswari, R.; Chin, W. W.; Ong, K. W.; Soo, K. C. Immune Response against Angiosarcoma Following Lower Fluence Rate Clinical Photodynamic Therapy. *J. Environ. Pathol. Toxicol. Oncol.* **2008**, *27*, 35–42.
7. Frangioni, J. V. *In Vivo* near-Infrared Fluorescence Imaging. *Curr. Opin. Chem. Biol.* **2003**, *7*, 626–634.
8. Zhang, P.; Steelant, W.; Kumar, M.; Scholfield, M. Versatile Photosensitizers for Photodynamic Therapy at Infrared Excitation. *J. Am. Chem. Soc.* **2007**, *129*, 4526–4527.
9. Qian, H. S.; Guo, H. C.; Ho, P. C.; Mahendran, R.; Zhang, Y. Mesoporous-Silica-Coated Up-Conversion Fluorescent Nanoparticles for Photodynamic Therapy. *Small* **2009**, *5*, 2285–2290.
10. Guo, H.; Qian, H.; Idris, N. M.; Zhang, Y. Singlet Oxygen-Induced Apoptosis of Cancer Cells Using Upconversion Fluorescent Nanoparticles as a Carrier of Photosensitizer. *Nanomedicine* **2010**, *6*, 486–495.
11. Idris, N. M.; Gnanasammandhan, M. K.; Zhang, J.; Ho, P. C.; Mahendran, R.; Zhang, Y. *In Vivo* Photodynamic Therapy Using Upconversion Nanoparticles as Remote-Controlled Nanotransducers. *Nat. Med.* **2012**, *18*, 1580–1585.
12. Chen, F.; Zhang, S.; Bu, W.; Chen, Y.; Xiao, Q.; Liu, J.; Xing, H.; Zhou, L.; Peng, W.; Shi, J. A Uniform Sub-50 nm-Sized Magnetic/Upconversion Fluorescent Bimodal Imaging Agent Capable of Generating Singlet Oxygen by Using a 980 nm Laser. *Chemistry* **2012**, *18*, 7082–7090.
13. Liu, K.; Liu, X.; Zeng, Q.; Zhang, Y.; Tu, L.; Liu, T.; Kong, X.; Wang, Y.; Cao, F.; Lambrechts, S. A.; *et al.* Covalently Assembled NIR Nanoplatform for Simultaneous Fluorescence Imaging and Photodynamic Therapy of Cancer Cells. *ACS Nano* **2012**, *6*, 4054–4062.
14. Zhou, A.; Wei, Y.; Wu, B.; Chen, Q.; Xing, D. Pyropheophorbide a and c(RGDyk) Comodified Chitosan-Wrapped Upconversion Nanoparticle for Targeted Near-Infrared Photodynamic Therapy. *Mol. Pharmaceutics* **2012**, *9*, 1580–1589.
15. Qiao, X. F.; Zhou, J. C.; Xiao, J. W.; Wang, Y. F.; Sun, L. D.; Yan, C. H. Triple-Functional Core-Shell Structured Upconversion Luminescent Nanoparticles Covalently Grafted with Photosensitizer for Luminescent, Magnetic Resonance Imaging and Photodynamic Therapy *In Vitro*. *Nanoscale* **2012**, *4*, 4611–4623.
16. Zhao, Z.; Han, Y.; Lin, C.; Hu, D.; Wang, F.; Chen, X.; Chen, Z.; Zheng, N. Multifunctional Core-Shell Upconverting Nanoparticles for Imaging and Photodynamic Therapy of Liver Cancer Cells. *Chem.—Asian J.* **2012**, *7*, 830–837.
17. Wang, C.; Tao, H.; Cheng, L.; Liu, Z. Near-Infrared Light Induced *In Vivo* Photodynamic Therapy of Cancer Based on Upconversion Nanoparticles. *Biomaterials* **2011**, *32*, 6145–6154.
18. Cui, S.; Chen, H.; Zhu, H.; Tian, J.; Chi, X.; Qian, Z.; Achilefu, S.; Gu, Y. Amphiphilic Chitosan Modified Upconversion Nanoparticles for *In Vivo* Photodynamic Therapy Induced by Near-Infrared Light. *J. Mater. Chem.* **2012**, *22*, 4861–4873.
19. Park, Y. I.; Kim, H. M.; Kim, J. H.; Moon, K. C.; Yoo, B.; Lee, K. T.; Lee, N.; Choi, Y.; Park, W.; Ling, D.; *et al.* Theranostic Probe Based on Lanthanide-Doped Nanoparticles for Simultaneous *In Vivo* Dual-Modal Imaging and Photodynamic Therapy. *Adv. Mater.* **2012**, *24*, 5755–5761.
20. Cui, S.; Yin, D.; Chen, Y.; Di, Y.; Chen, H.; Ma, Y.; Achilefu, S.; Gu, Y. *In Vivo* Targeted Deep-Tissue Photodynamic Therapy Based on near-Infrared Light Triggered Upconversion Nanoconstruct. *ACS Nano* **2013**, *7*, 676–688.
21. Kubota, Y.; Shuin, T.; Kawasaki, C.; Hosaka, M.; Kitamura, H.; Cai, R.; Sakai, H.; Hashimoto, K.; Fujishima, A. Photokilling of T-24 Human Bladder Cancer Cells with Titanium Dioxide. *Br. J. Cancer* **1994**, *70*, 1107–1111.
22. Zhang, A. P.; Sun, Y. P. Photocatalytic Killing Effect of TiO_2 Nanoparticles on Ls-174-T Human Colon Carcinoma Cells. *World J. Gastroenterol.* **2004**, *10*, 3191–3193.
23. Lagopati, N.; Kitsiou, P. V.; Kontos, A. I.; Venieratos, P.; Kotsopoulou, E.; Kontos, A. G.; Dionysiou, D. D.; Pispas, S.; Tsilibary, E. C.; Falaras, P. Photo-Induced Treatment of Breast Epithelial Cancer Cells Using Nanostructured Titanium Dioxide Solution. *J. Photochem. Photobiol., A* **2010**, *214*, 215–223.
24. Wang, C.; Cao, S.; Tie, X.; Qiu, B.; Wu, A.; Zheng, Z. Induction of Cytotoxicity by Photoexcitation of TiO_2 Can Prolong Survival in Glioma-Bearing Mice. *Mol. Biol. Rep.* **2011**, *38*, 523–530.

25. Rozhkova, E. A.; Ulasov, I.; Lai, B.; Dimitrijevic, N. M.; Lesniak, M. S.; Rajh, T. A High-Performance Nanobio Photocatalyst for Targeted Brain Cancer Therapy. *Nano Lett.* **2009**, *9*, 3337–3342.
26. Cai, R.; Kubota, Y.; Shuin, T.; Sakai, H.; Hashimoto, K.; Fujishima, A. Induction of Cytotoxicity by Photoexcited TiO_2 Particles. *Cancer Res.* **1992**, *52*, 2346–2348.
27. Xu, Q. C.; Zhang, Y.; Tan, M. J.; Liu, Y.; Yuan, S.; Choong, C.; Tan, N. S.; Tan, T. T. Anti-Cangptl4 Ab-Conjugated N-TiO(2) / NaYF(4):Yb,Tm Nanocomposite for near Infrared-Triggered Drug Release and Enhanced Targeted Cancer Cell Ablation. *Adv. Healthcare Mater.* **2012**, *1*, 470–474.
28. Idris, N. M.; Lucky, S. S.; Li, Z.; Huang, K.; Zhang, Y. Photoactivation of Core-Shell Titania Coated Upconversion Nanoparticles and Their Effect on Cell Death. *J. Mater. Chem. B* **2014**, *2*, 7017–7026.
29. Suttiponparnit, K.; Jiang, J.; Sahu, M.; Suvachittanont, S.; Charinpanitkul, T.; Biswas, P. Role of Surface Area, Primary Particle Size, and Crystal Phase on Titanium Dioxide Nanoparticle Dispersion Properties. *Nanoscale Res. Lett.* **2011**, *6*, 27.
30. Qi, L.; Xu, Z.; Jiang, X.; Hu, C.; Zou, X. Preparation and Antibacterial Activity of Chitosan Nanoparticles. *Carbohydr. Res.* **2004**, *339*, 2693–2700.
31. Lundqvist, M.; Stigler, J.; Elia, G.; Lynch, I.; Cedervall, T.; Dawson, K. A. Nanoparticle Size and Surface Properties Determine the Protein Corona with Possible Implications for Biological Impacts. *Proc. Natl. Acad. Sci. U. S. A.* **2008**, *105*, 14265–14270.
32. Klinger, A.; Steinberg, D.; Kohavi, D.; Sela, M. N. Mechanism of Adsorption of Human Albumin to Titanium *In Vitro*. *J. Biomed. Mater. Res.* **1997**, *36*, 387–392.
33. Aggarwal, P.; Hall, J. B.; McLeland, C. B.; Dobrovolskaia, M. A.; McNeil, S. E. Nanoparticle Interaction with Plasma Proteins as It Relates to Particle Biodistribution, Biocompatibility and Therapeutic Efficacy. *Adv. Drug Delivery Rev.* **2009**, *61*, 428–437.
34. Wolfram, J.; Yang, Y.; Shen, J.; Moten, A.; Chen, C.; Shen, H.; Ferrari, M.; Zhao, Y. The Nano-Plasma Interface: Implications of the Protein Corona. *Colloids Surf., B* **2014**, 10.1016/j.colsurfb.2014.02.035.
35. Vonarbourg, A.; Passirani, C.; Saulnier, P.; Benoit, J. P. Parameters Influencing the Stealthiness of Colloidal Drug Delivery Systems. *Biomaterials* **2006**, *27*, 4356–4373.
36. Owens, D. E., 3rd; Peppas, N. A. Opsonization, Biodistribution, and Pharmacokinetics of Polymeric Nanoparticles. *Int. J. Pharm.* **2006**, *307*, 93–102.
37. Jokerst, J. V.; Lobovkina, T.; Zare, R. N.; Gambhir, S. S. Nanoparticle Pegylation for Imaging and Therapy. *Nanomedicine* **2011**, *6*, 715–728.
38. Sakhtianchi, R.; Minchin, R. F.; Lee, K.-B.; Alkilany, A. M.; Serpooshan, V.; Mahmoudi, M. Exocytosis of Nanoparticles from Cells: Role in Cellular Retention and Toxicity. *Adv. Colloid Interface Sci.* **2013**, *201−202*, 18–29.
39. Bae, Y. M.; Park, Y. I.; Nam, S. H.; Kim, J. H.; Lee, K.; Kim, H. M.; Yoo, B.; Choi, J. S.; Lee, K. T.; Hyeon, T.; *et al.* Endocytosis, Intracellular Transport, and Exocytosis of Lanthanide-Doped Upconverting Nanoparticles in Single Living Cells. *Biomaterials* **2012**, *33*, 9080–9086.
40. Li, T.; Takeoka, S. A Novel Application of Maleimide for Advanced Drug Delivery: *In Vitro* and *In Vivo* Evaluation of Maleimide-Modified pH-Sensitive Liposomes. *Int. J. Nanomed.* **2013**, *8*, 3855–3866.
41. Li, T.; Takeoka, S. Enhanced Cellular Uptake of Maleimide-Modified Liposomes *via* Thiol-Mediated Transport. *Int. J. Nanomed.* **2014**, *9*, 2849–2861.
42. Ripamonti, F.; Albano, L.; Rossini, A.; Borrelli, S.; Fabris, S.; Mantovani, R.; Neri, A.; Balsari, A.; Magnifico, A.; Tagliabue, E. EGFR through Stat3Modulates Δn63α Expression to Sustain Tumor-Initiating Cell Proliferation in Squamous Cell Carcinomas. *J. Cell. Physiol.* **2013**, *228*, 871–878.
43. Buytaert, E.; Dewaele, M.; Agostinis, P. Molecular Effectors of Multiple Cell Death Pathways Initiated by Photodynamic Therapy. *Biochim. Biophys. Acta, Rev. Cancer* **2007**, *1776*, 86–107.
44. Mroz, P.; Yaroslavsky, A.; Kharkwal, G. B.; Hamblin, M. R. Cell Death Pathways in Photodynamic Therapy of Cancer. *Cancers* **2011**, *3*, 2516–2539.
45. Henderson, B. W.; Dougherty, T. J. How Does Photodynamic Therapy Work?. *Photochem. Photobiol.* **1992**, *55*, 145–157.
46. Dolmans, D. E. J. G. J.; Fukumura, D.; Jain, R. K. Photodynamic Therapy for Cancer. *Nat. Rev. Cancer* **2003**, *3*, 380–387.
47. Oleinick, N. L.; Morris, R. L.; Belichenko, I. The Role of Apoptosis in Response to Photodynamic Therapy: What, Where, Why, and How. *Photochem. Photobiol. Sci.* **2002**, *1*, 1–21.
48. Li, Z.; Zhang, Y. An Efficient and User-Friendly Method for the Synthesis of Hexagonal-Phase NaYF4:Yb, Er/Tm Nanocrystals with Controllable Shape and Upconversion Fluorescence. *Nanotechnology* **2008**, *19*, 345606.
49. Li, Z.; Zhang, Y.; Jiang, S. Multicolor Core/Shell-Structured Upconversion Fluorescent Nanoparticles. *Adv. Mater.* **2008**, *20*, 4765–4769.